Conductive 3D microstructures by direct 3D printing of polymer/carbon nanotube nanocomposites *via* liquid deposition modeling

Giovanni Postiglione, Gabriele Natale, Gianmarco Griffini *, Marinella Levi, Stefano Turri

Department of Chemistry, Materials and Chemical Engineering "Giulio Natta", Politecnico di Milano, Piazza Leonardo da Vinci 32, 20133 Milano, Italy

Received 7 November 2014
Received in revised form 15 May 2015
Accepted 17 May 2015
Available online 27 May 2015

1. Introduction

Three-dimensional (3D) printing is a fabrication technology that consists in the creation of a 3D object starting from a digital model. 3D printing technologies have evolved very rapidly in recent years and have shifted apart from their traditional application field, namely rapid prototyping. Indeed, 3D printing is now being used routinely in a variety of manufacturing sectors ranging from aerospace and automotive to bioengineering [1,2]. At present, stereolithography, selective laser sintering, selective laser melting and fused deposition modeling (FDM) are among the most widely employed and investigated additive manufacturing methods both in academia and in industrial environments [3]. The various 3D printing technologies differ in terms of cost, maximum spatial resolution and type of materials used. In particular, for the first three methods, 3D features with a very high spatial resolution (in the order of a few μm at most) have been demonstrated but at the expense of relatively high equipment costs and the need of specialized personnel to operate them [3,4]. On the other hand, FDM has recently become fairly popular especially among non-specialized personnel as it represents a very cost effective approach to produce 3D objects with a relatively good resolution, which can approach 40 μm [5]. However, being a thermally-driven process that requires melting of a thermoplastic filament prior to the additive deposition of the extruded feature, it exhibits some limitations related to the materials to deposit, as only relatively few polymers possess the right thermal and rheological properties to be easily processable with this technology (with poly(lactic acid) – PLA and acrylonitrile–butadiene–styrene – ABS being among the most widely employed) [6]. Recently, the FDM approach was shown to allow a high degree of orientation of short reinforcing fibers in polymer-based composites during filament extrusion, resulting in 3D printed components with unique structural properties that can significantly exceed those of traditional compression molded samples [7]. In addition, the potential of the FDM technology for the fabrication of electronic sensors was recently demonstrated by 3D-printing solid filaments obtained starting from a dispersion of conductive carbon black into a solution of a commercial formulation of poly(caprolactone) (PCL) in dichloromethane (DCM) followed by evaporation of the solvent to form the solid filament to be extruded in a table-top FDM 3D printer [8]. Even though the approach presented in this work clearly allows the possibility to 3D-print objects with embedded sensors and electronic functionalities in a relatively simple fashion, it still requires the additional step of the production of a solid (nano)composite filament to be heated and melted in order to be processed with a standard FDM 3D printer.

Very recently solvent-cast 3D printing has emerged as a versatile and cost-effective strategy to overcome some of the limits imposed by the FDM approach [9]. This relatively new technology consists in the additive deposition of material layers directly from a solution in

* Corresponding author. Tel.: +39 02 2399 3213.
E-mail address: gianmarco.griffini@polimi.it (G. Griffini).

a volatile solvent. By means of this technology, the production of freeform structures, scaffolds and other self-standing microstructures was recently demonstrated using a computer-controlled robot moving along the *x*, *y* and *z* axes a dispensing apparatus equipped with a 100 μm inner-diameter extruding nozzle, starting from a concentrated solution of PLA in DCM [9]. In addition, by sputtering a metallic layer a few tens of μm thick onto the 3D printed structure, electrically conducting objects could also be obtained. However, no examples of the fabrication of intrinsically conductive 3D microstructures *via* direct 3D printing of conductive polymer-based nanocomposite materials from liquid dispersion have so far been reported in the literature, notwithstanding their enormous technological potential for application in fields such as microelectronics and biomedical engineering, where this approach would allow the direct fabrication of conductive microstructures with tailored 3D architectures in a low-cost and highly versatile fashion.

In the effort to address this issue, a 3D printing technique is developed in this work for the fabrication of conductive 3D microstructures with arbitrary shapes *via* the deposition of a new conductive nanocomposite from liquid dispersion by means of a low-cost commercial benchtop 3D printer equipped with a syringe dispenser (see Supplementary data). This method, that will be called liquid deposition modeling (LDM) throughout the text in analogy to the FDM approach introduced earlier, is based on the direct deposition of a homogeneous dispersion of multiwall carbon nanotubes (MWCNTs) in PLA using a high volatility solvent (i.e., DCM) as dispersion medium to ensure fast evaporation during wet filament deposition and rapid formation of rigid 3D microstructures. A thorough electrical characterization of the nanocomposite at increasing MWCNT concentrations is performed to evaluate the percolation threshold to achieve electrical conductivity. In addition, the rheological behavior of the nanocomposite dispersion is experimentally investigated at varying solid (PLA) content and a printability window for this system is identified based on the shear-rate of the material at the extrusion nozzle. Finally, examples of conductive 3D microstructures directly formed upon LDM of such MWCNT-based nanocomposite dispersion are presented. Conductive features as small as 100 μm can be reproducibly obtained with this method, indicating the high reliability of our approach. LDM clearly lends itself to the possibility of incorporating different types of structural and functional (nano)fillers in the 3D printed extruded feature without the need of producing a solid (nano)composite filament, thus presenting clear benefits compared to the more common FDM approach.

2. Experimental

MWCNTs were purchased from Nanocyl, Belgium (Nanocyl NC 3100, purity >95%, 9.5 nm average diameter and 1.5 μm average length). PLA pellets were supplied by Futura Elettronica, Italy. DCM was purchased from Sigma–Aldrich, Italy. All products were used as received. For the preparation of the nanocomposite dispersions at increasing MWCNT concentration, a 3 wt% stock solution of PLA in DCM was prepared under magnetic stirring at room temperature for 3 h. After complete dissolution of PLA, the desired amount of MWCNTs (ranging from 0.5 wt% to 10 wt% in PLA) was dispersed in the PLA/DCM solution using the following procedure [10]: addition of the MWCNTs, 30 min magnetic stirring at 950 rpm, 1 h ultrasonic bath (Starsonic 90) at room temperature, 30 min ultrasonication with a Sonic & Materials VCX130 sonicator tip (20 kHz, 130 W, oscillation amplitude 80%). This last step was carried out in an ice bath in order to prevent DCM evaporation and to minimize undesired exothermic phenomena resulting from the ultrasonication process. A similar procedure was employed for the preparation of nanocomposite dispersions at increasing PLA concentrations in DCM. In this case, a 1 wt% MWCNT concentration in PLA was employed and the PLA content in DCM was progressively varied (25 wt%, 30 wt% and 35 wt%). To perform electrical measurements, 25 mm × 75 mm thin film samples with a thickness ranging between 40 and 100 μm were prepared by drop-casting each nanocomposite dispersion with a given MWCNT concentration on a glass substrate. Upon drying in a ventilated oven, a solid self-standing nanocomposite film was obtained. The electrical conductivity of the nanocomposite films was measured using a four-point probe apparatus connected to a Keithley 2612 digital source-measure unit. A current scan between 0.01 and 0.1 A was applied on each sample with 50 steps and a settling time of 1 s for each measured step. The electrical conductivity of the nanocomposites was then calculated from resistance measurements [11]. Characterization of the rheological properties of the nanocomposite dispersions at increasing PLA concentrations (1 wt% MWCNT in PLA) was performed using a Rheometrics DSR200 rheometer with a 25 mm plate–cone configuration at 25 °C. Steady shear tests on the MWCNT/PLA/DCM dispersions were performed for 3 min in the 0–4500 Pa range. Optical microscopy was employed to evaluate the microstructural features of the 3D-printed architectures using an Olympus BX-60 reflected-light optical microscope with bright-field (BF) and dark-field (DF) imaging equipped with an Infinity 2 digital camera. Scanning electron microscopy (SEM) was performed on 3D-printed nanocomposite-based microstructures with a Carl Zeiss EVO 50 Extended Pressure scanning electron microscope (acceleration voltage of 15.00–17.50 kV) to evaluate their surface morphology and the 3D architecture (samples were sputtered with a gold coating prior to SEM analysis). A low-cost home-assembled 3Drag 1.2 benchtop printer (Futura Elettronica, Italy) was used for LDM-based 3D printing of the conductive nanocomposite microstructures (see Supplementary data for details on the 3D printer setup).

3. Results and discussion

In this work, the high electrical conductivity of MWCNTs was exploited to impart conductive character to the final MWCNT/PLA nanocomposite. To determine the effect of the addition of MWCNTs to the PLA matrix, the volume electrical conductivity σ of MWCNT/PLA nanocomposites was evaluated from resistance measurements on solvent-cast nanocomposite films with increasing MWCNT content (0.5–10 wt%). As shown in Fig. 1a, conductivity σ is found to increase substantially with respect to pristine PLA already upon addition of 0.5 wt% MWCNTs. Furthermore, a progressive increase in σ is observed for increasing MWCNT concentrations following a typical percolation behavior, until values in the range 10–100 S/m are reached for highly concentrated (5–10 wt%) MWCNT/PLA nanocomposites. Similar values of electrical conductivity were obtained on analogous nanocomposite systems based on MWCNTs and PLA matrix [12,13].

Achieving a uniform homogeneous dispersion of MWCNTs within a polymeric matrix is a key factor for the development of printable MWCNT-based nanocomposites because of the high tendency of MWCNTs to form bundles and aggregates [14] that may cause clogging of the printing nozzle and flux instability during the printing process. Therefore, an appropriate MWCNT concentration is required to obtain a nanocomposite material that is simultaneously conductive and 3D printable. The fracture surface of cryo-fractured 3D printed MWCNT/PLA nanocomposites containing 10 wt% of MWCNTs obtained from SEM analysis is shown in Fig. 1b. As evident from the SEM micrograph, a good level of dispersion and distribution of MWCNTs (white dots in the image) is achieved in the PLA matrix without the formation of any noticeable

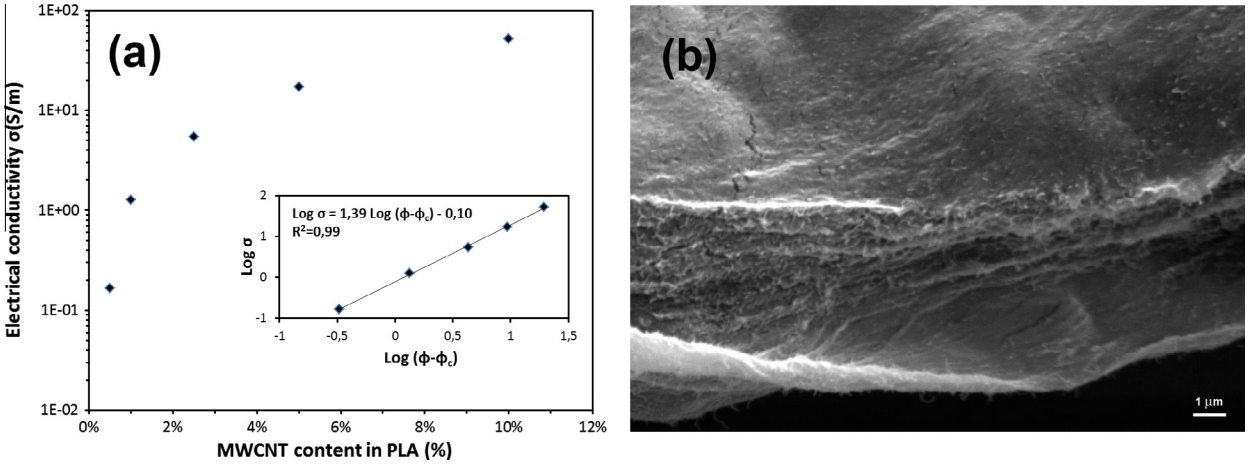

Fig. 1. (a) Volume electrical conductivity as a function of MWCNT concentration. The inset shows the log–log plot of the electrical conductivity versus the volume fraction of MWCNTs; (b) SEM micrograph of cryo-fractured 3D-printed MWCNT/PLA nanocomposites (10 wt% MWCNT in PLA). (For interpretation of the references to color in this figure legend, the reader is referred to the web version of this article.)

aggregates, even at high MWCNT content. With the aim of determining the minimum theoretical MWCNT concentration to achieve electrical conductivity in the nanocomposite system, the electrical percolation threshold for the MWCNT/PLA nanocomposite system was evaluated using the following power law [15]:

$$\sigma \propto (\varphi - \varphi_c)^{\alpha} \quad (1)$$

where σ is the electrical conductivity, φ is the MWCNT volume concentration in the nanocomposite, φ_c is the critical MWCNT volume concentration at electrical percolation and α is a critical exponent. An excellent fit to the experimental values of $\log(\sigma)$ versus $\log(\varphi - \varphi_c)$ was obtained by a MWCNT percolation threshold concentration of 0.67 wt% and $\alpha = 1.39$, as shown in the inset to Fig. 1a. These values are in agreement with recently reviewed data on polymer-based nanocomposites, in which α values between 1.3 and 4 and φ_c well below 1 wt% are commonly found for systems containing MWCNTs [16]. Despite electrical measurements in this work were conducted on cast nanocomposite films, it is worth pointing out that the percolation threshold values obtained herein should represent an underestimate of the actual electrical behavior found in 3D printed filaments. Indeed, it was shown that the percolation conductivity of the nanocomposite may also be affected by the shearing at the nozzle tip due to shear-induced alignment of the MWCNT [17]. In addition to optimizing the electrical properties of the MWCNT/PLA nanocomposites, their rheological behavior needs to be thoroughly analyzed. Indeed, in the LDM-based 3D printing process the rheological profile of the nanocomposite dispersion critically determines its ability to flow through the printing nozzle and thus influences its actual printability into stable 3D solid microstructures. To this end, the viscosity of nanocomposite dispersions with varying PLA/DCM weight ratio (25/75, 30/70, 35/65) and fixed MWCNT concentration (1 wt% in PLA) was determined by isothermal cone–plate rheological measurements and the results are presented in Fig. 2. All nanocomposite dispersions clearly exhibited a typical shear-thinning behavior characterized by decreasing viscosity with increasing shear rate. In addition, an increase in viscosity is found upon addition of MWCNT. This rheological response is highly desirable in the context of LDM-based 3D printing as it allows to enhance nanocomposite processability through the capillary nozzle under the high shear-rates typical of the extrusion process due to the decreased viscosity of the material.

In order to determine the correct printability window of the nanocomposite dispersions investigated, the process-related wall shear-rate and wall shear-stress were estimated using the capillary flow model (see Supplementary data for details on the calculations) [18,19]. As a result, an allowable process-related shear-stress interval for a given material could also be estimated as a function of the printing-speed (*viz.*, shear-rate) settings. Accordingly, plots of the process-related shear-stress τ as a function of the process-related shear-rate $\dot{\gamma}$ for the different MWCNT/PLA nanocomposite dispersions investigated in this work were constructed and presented in Fig. 2b, where the corresponding above mentioned printability windows are also shown. As evident from Fig. 2b, the rheological curve of the highly concentrated C1-PLA35 system (35 wt% PLA in DCM, 1 wt% MWCNTs) is completely outside its printability window, indicating that a minimum extruding pressure (minimum applied shear-stress τ) higher than the maximum pressure attainable by the printing machine P_a (maximum allowable shear-stress τ_{max}) is required to process such system. This means that the viscosity of such nanocomposite dispersion is not compatible with our printing system. On the other hand, C1-PLA30 and C1-PLA25 dispersions (1 wt% MWCNTs – 30 wt% and 25 wt% PLA in DCM, respectively) showed a finite overlap between the process-related shear-stress curve of the material and its printability window, indicating that printing of these nanocomposite systems can be accomplished, provided that the appropriate combination of processing conditions (namely, shear-rate and shear-stress) are employed. In particular, it is evident from Fig. 2b that C1-PLA30 only allows for a very short range of useful shear-rates ($\dot{\gamma}$ = 5–11 s^{-1}, low printing speeds) while C1-PLA25 is characterized by a much broader $\dot{\gamma}$ printability range (higher printing speeds). These differences can be attributed to the different rheological response of these two systems at high shear-rates, as also evident from Fig. 2a. These results were confirmed by printing experiments of these nanocomposite systems directly performed with the 3D printing apparatus. Although the C1-PLA25 system offered a wider range of printing speeds, the best results in terms of resolution of 3D printed features at constant printing settings were obtained by processing the C1-PLA30 system at very low printing speeds (i.e., 0.1 mm s^{-1}, $\dot{\gamma}$ = 10 s^{-1}), likely due to the lower amount of solvent present in this case.

In order to demonstrate the potential of LDM-based 3D printing of conductive MWCNT-based nanocomposite systems, different microstructures were fabricated using a low-cost benchtop 3D printer appropriately modified to accommodate a pressure-activated syringe (see Supplementary data) feeding the extruding nozzle with the MWCNT/PLA nanocomposite dispersions (Fig. 3). First, a woven-like microstructure was obtained by depositing two layers of materials on top of each other. In order

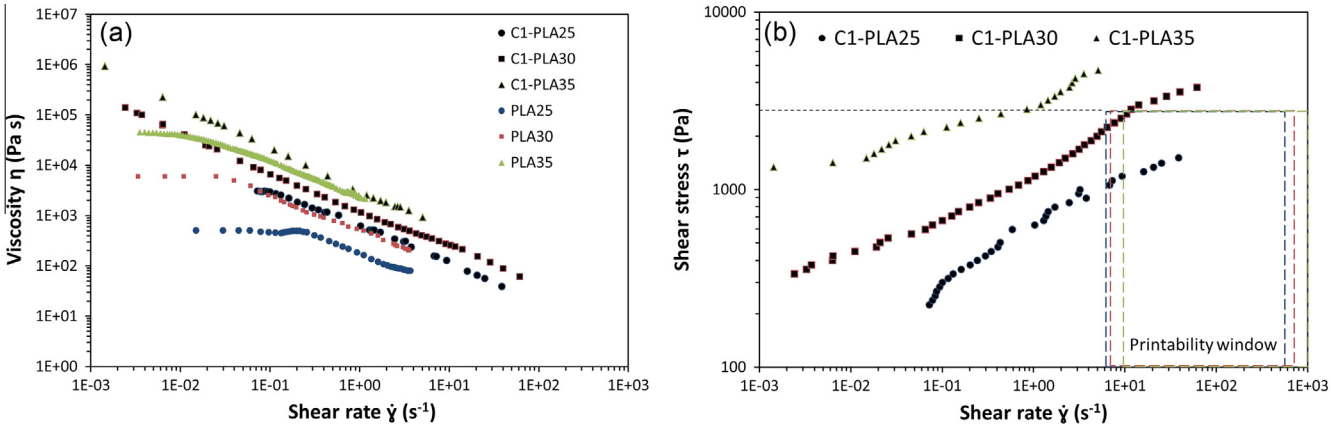

Fig. 2. (a) Viscosity and flow curves for neat PLA and MWCNT/PLA nanocomposite dispersions at increasing PLA concentration in DCM; (b) shear-stress as a function of shear-rate for the MWCNT/PLA nanocomposite dispersions at increasing PLA concentrations in DCM (25 wt% (C1-PLA25), 30 wt% (C1-PLA30) and 35 wt% (C1-PLA35) – the corresponding printability windows are also presented as the areas within the dashed lines). (For interpretation of the references to color in this figure legend, the reader is referred to the web version of this article.)

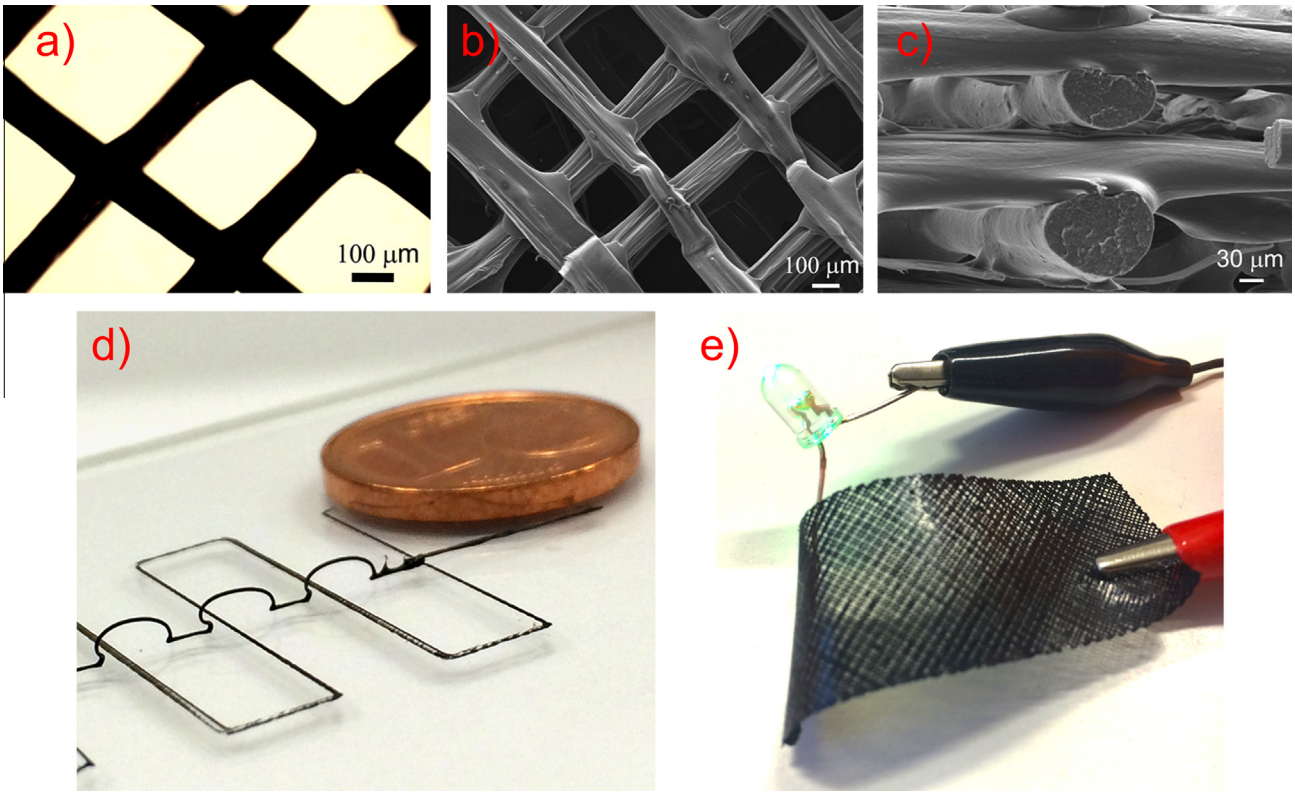

Fig. 3. (a) Top-view optical microscopy image of a LDM-based3D printed two-layer woven-like microstructure; SEM (b) top and (c) side view images of a representative ten-layer scaffold; (d) optical photograph of a LDM-based 3D printed filament deposited in a freeform manner (a 1 cent euro coin is reported in the image for dimensional reference); (e) 3D printed MWCNT-based nanocomposite woven structure used as conductive element in a simple electrical circuit. (For interpretation of the references to color in this figure legend, the reader is referred to the web version of this article.)

to do so, the C1-PLA30 nanocomposite system was employed, at a printing speed of 0.1 mm s^{-1} ($\dot{\gamma} = 7\ s^{-1}$). As shown in the optical micrograph presented in Fig. 3a, the wet MWCNT/PLA nanocomposite filament extrusion resulted in planar solid features of 100 μm average width. The same printing process parameters (0.1 mm s^{-1} printing speed) and MWCNT-PLA nanocomposite system (C1-PLA30) were used to fabricate a 3D-printed ten-layer scaffold. As shown in Fig. 3b and c where the SEM images of different regions of a representative 3D-printed scaffold are presented, a comparable feature resolution (100 μm) as that obtained in the 2D woven-like microstructure presented in Fig. 3a could be achieved. In addition, the stability of the as-formed solid nanocomposite filament allows to fabricate 3D features spanning over a few hundreds μm, as evident from Fig. 3b. Furthermore, the scaffold side-view reveals the characteristic circular cross-section of the extruded filament of approximately 100 μm (Fig. 3c) of diameter, which is maintained even in the presence of multiple overlying layers. Fig. 3d presents an example of a freeform 3D microstructure

in which a 100 μm diameter solid filament allows to achieve spanning self-standing features covering a few mm in length repetitively. In this case, C1-PLA25 system was employed at 5 mm s^{-1} ($\dot{\gamma}$ = 315 s^{-1}), so as to be able to speed-up the 3D printing process, induce rapid solvent evaporation and allow the formation of the spanning features. Such 3D microstructures suggest the possibility of employing these LDM-based 3D-printed architectures to fabricate conductive electronic components at the microscale in a very versatile fashion. To this end, a 75 mm × 25 mm free-standing and flexible woven structure was fabricated by means of the proposed LDM technology (Fig. 3e) and it was employed to set up a simple electrical circuit to turn on a commercial green LED by means of a 3 V CR2032-type watch battery, thus giving a further practical demonstration of the potential applicability of these fully-functional conductive microstructured systems in the field of microelectronics.

4. Conclusions

In summary, the fabrication of conductive 3D microstructures with arbitrary shapes is demonstrated by means of a new LDM 3D printing method based on the solvent-assisted additive deposition of a conductive nanocomposite using a modified low-cost benchtop 3D printer. Characterization of the electrical properties of the materials at increasing MWCNT concentrations evidenced a significant increase in the electrical conductivity of the nanocomposite with respect to the pristine PLA matrix material. Values of electrical conductivity in the 10–100 S/m range were obtained for high (>5 wt%) MWCNT concentrations, with a percolation threshold concentration of 0.67 wt%. Characterization of the rheological properties of the nanocomposite dispersions at varying PLA content was performed and printability windows for these systems were identified based on the estimation of the shear-rate of the dispersion at the extrusion nozzle. Finally, examples of spanning and self-supported conductive 3D microstructures directly formed upon LDM-based 3D printing of such MWCNT-based nanocomposite dispersions were presented. Conductive features as small as 100 μm could be reproducibly obtained with our method, demonstrating the high reliability of our approach. To the best of our knowledge, this represents the first demonstration of direct additive layer deposition of intrinsically conductive 3D microstructures from polymeric nanocomposite materials by means of a low-cost 3D printing technique based on the LDM approach. The results of this study clearly demonstrate the technological potential of conductive nanocomposite LDM-based 3D printing that may enable the integration of electronic functionalities into complex 3D objects in a straightforward and versatile fashion.

Appendix A. Supplementary material

Supplementary data associated with this article can be found, in the online version.

References

[1] Gross BC, Erkal JL, Lockwood SY, Chen C, Spence DM. Evaluation of 3D printing and its potential impact on biotechnology and the chemical sciences. Anal Chem 2014;86:3240–53.
[2] Petrovic V, Haro Gonzalez JV, Jordá Ferrando O, Delgado Gordillo J, Blasco Puchades JR, Portoles Griñan L. Additive layered manufacturing: sectors of industrial application shown through case studies. Int J Prod Res 2011;49:1061–79.
[3] Gibson I, Rosen DW, Stucker B. Additive manufacturing technologies – Rapid prototyping to direct digital manufacturing. Springer; 2010.
[4] Farahani RD, Chizari K, Therriault D. Three-dimensional printing of freeform helical microstructures: a review. Nanoscale 2014;6:10470–85.
[5] Yamada A, Niikura F, Ikuta K. A three-dimensional microfabrication system for biodegradable polymers with high resolution and biocompatibility. J Micromech Microeng 2008;18:025035.
[6] Monzón MD, Gibson I, Benítez AN, Lorenzo L, Hernández PM, Marrero MD. Process and material behavior modeling for a new design of micro-additive fused deposition. Int J Adv Manuf Technol 2013;67:2717–26.
[7] Tekinalp HL, Kunc V, Velez-Garcia GM, Duty CE, Love LJ, Naskar AK, et al. Highly oriented carbon fiber–polymer composites via additive manufacturing. Compos Sci Technol 2014;105:144–50.
[8] Leigh SJ, Bradley RJ, Purssell CP, Billson DR, Hutchins DA. A Simple, low-cost conductive composite material for 3D printing of electronic sensors. PLoS ONE 2012;7:e49365.
[9] Guo S-Z, Gosselin F, Guerin N, Lanouette A-M, Heuzey M-C, Therriault D. Solvent-cast three-dimensional printing of multifunctional microsystems. Small 2013;9:4118–22.
[10] Molina D, Griffini G, Levi M, Turri S. Novel conductive nanocomposites from perfluoropolyether waterborne polyurethanes and carbon nanotubes. Polym Adv Technol 2014;25:1082–8.
[11] ASTM Designation: F 84–99, Standard test method for measuring resistivity of silicon wafers with an in-line four-point probe.
[12] Mai F, Habibi Y, Raquez J-M, Dubois P, Feller J-F, Peijs T, et al. Poly(lactic acid)/carbon nanotube nanocomposites with integrated degradation sensing. Polymer 2013;54:6818–23.
[13] Moon S-I, Jin F, Lee C-j, Tsutsumi S, Hyon S-H. Novel carbon nanotube/poly(L-lactic acid) nanocomposites: their modulus, thermal stability, and electrical conductivity. Macromol Symp 2005;224:287–95.
[14] Ma P-C, Siddiqui NA, Marom G, Kim J-K. Dispersion and functionalization of carbon nanotubes for polymer-based nanocomposites: a review. Compos A 2010;41:1345–67.
[15] Balberg I. A comprehensive picture of the electrical phenomena in carbon black polymer composites. Carbon 2002;40:139–43.
[16] Bauhofer W, Kovacs JZ. A review and analysis of electrical percolation in carbon nanotube polymer composites. Compos Sci Technol 2009;69:1486–98.
[17] Du F, Fischer JE, Winey KI. Effect of nanotube alignment on percolation conductivity in carbon nanotube/polymer composites. Phys Rev B 2005;72:121404.
[18] Barnes HA, Hutton JF, Walters K. An introduction to rheology. Elsevier; 1997.
[19] Pidcock GC, in het Panhuis M. Extrusion printing of flexible electrically conducting carbon nanotube networks. Adv Mater 2012;22:4790–800.